IEEE Access
Multidisciplinary ⋮ Rapid Review ⋮ Open Access Journal

Received 6 October 2023, accepted 22 October 2023, date of publication 30 October 2023, date of current version 16 November 2023.

Digital Object Identifier 10.1109/ACCESS.2023.3328555

RESEARCH ARTICLE

Curvature-Based Machine Vision Method for Measuring the Dimension of Ball Screws

YIJIA CHEN[1], YAO YAO[1], HAO YANG[1], YUE WU[2], KUNPENG ZHANG[1], AND XIAOMING PAN[1]

[1]College of Mechanical and Electrical Engineering, Wenzhou University, Wenzhou 325035, China
[2]College of Urban Transportation and Logistics, Shenzhen Technology University, Shenzhen 518118, China

Corresponding author: Xiaoming Pan (12944698@qq.com)

This work was supported in part by the Wenzhou Municipal Key Science and Research Program under Grant ZG2020029 and Grant ZG2022026.

ABSTRACT As a linear actuator, accurate dimension measurement is crucial to the transmission reliability and interchangeability of ball screws. However, most of the current approaches are ineligible for rapid ball screw in-situ inspections due to the installation condition requirement of the production line. In this research, a machine vision method is presented to achieve highly accurate measurements of crucial parameters (the center distance and raceway arcs) in ball screws using a curvature edge detection algorithm. To capture images of the immediate area surrounding the area of interest, a telecentric lens is used. Thereafter, the curvature-based edge detection algorithm is employed to extract the contours. The measurement location on the object is automatically chosen by using a shape-matching algorithm. Additionally, random noise is suppressed by using the multiple-measurement averaging technique. Based on the results of the experiments, it is concluded that the center distance and the two raceway arcs computed absolute errors are 0.0019 mm, 0.0055 mm, and 0.0059 mm, respectively.

INDEX TERMS Ball screw, curvature, edge detection, machine vision, shape matching.

I. INTRODUCTION

Aball screw is a linear actuator frequently used to convert rotary motion into linear motion and achieved remarkable success in high-precision mechanical transmission [1]. As a precision mechanical component, the ball screw is reported to have high stiffness, high transmission accuracy, and low sensitivity to variation [2]. It is reported that the drive torque needed for a ball screw is only one-third that of a conventional sliding screw [3]. Therefore, the ball screw is one of the most suitable transmission methods for saving drive motor power and has been widely utilized in several crucial applications [4], [5]. The typical structure of ball screws can be seen in Figure 1. The circulate rolling of the balls converts the rotational motion of the screw into the linear motion of the nut. As illustrated in the figure, the raceway arcs (dashed curve) radius nonconformity strongly influences the ball contact condition. Researchers have also demonstrated that ball screw quality is directly related to product performance [1], [6]. Therefore, accurate manufacturing error (dimensional error) evaluation is essential to maintain the performance of ball screws during the quality inspection process.

As a determining factor in mechanical performance improvement [7], there are several excellent reviews in the literature that pertain to ball screw geometrical measurement. Thread gauges and probes are the most widely used methods to estimate the machining accuracy of ball screws [8], [9]. When using go/no-go gauges, the ball screw dimensional conformity is verified whether the mating parts can cross the go gauge and be prevented by the no-go gauge. The probe method is also a common contact method for ball screw thread profile inspection. The ball screw's dimensional quality can be assessed by recording the vertical deflection of the stylus as it passes over the routes on the surface under investigation (a similar structure can be found in [10]). However, these contact inspection methods have certain disadvantages: (i) they are time-consuming, (ii) they create

The associate editor coordinating the review of this manuscript and approving it for publication was Jingang Jiang.

inevitable scratches, and (iii) they have limited capability for in-situ measurement.

A considerable of research has been done on non-contact on measuring for industrial parts, including stereopsis, light curtain, and grating projection profilometry [11], [12]. Stereopsis is a depth-sensing technique that takes advantage of the difference (or disparity) between two cameras [13]. A light curtain, which is supplied as a pair of receivers and transmitters can also be used to measure object dimensions [1]. Besides, grating projection profilometry is a type of structured light system that uses a phase-shifting algorithm to gather object height data and has been successfully applied in ball screw inspections [14]. However, cause of the complex accessories contained in these methods, developing a portable system suitable for in-situ ball screw measurements remains difficult. With the aid of digital image processing and the increase in computational power, machine vision has become a popular method for dimensional measurements because of its flexibility and high speed [15]. To obtain highly accurate measurements of the sizes of the bayonets on large automotive brake pads, Xiang et al. [16] proposed a measurement method based on a two-camera machine vision system. Gong and Seibel [17] proposed a small inner surface profiler using a feature-based three-dimensional panoramic registration. With a digital single lens reflex camera, Lee et al. [18] developed a machine vision-based in-process insert wear detection method and offers exciting opportunities to inspect the ball screw.

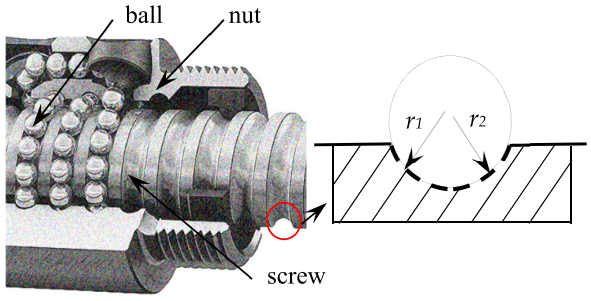

FIGURE 1. General ball screw structure.

Motivated by the idea of Lee et al. [18], a method for achieving accurate in-situ measurements of ball screw key parameters using machine vision technology is presented in this research. The method uses only one camera (with a telecentric lens) to capture local images around the region of interest (ROI); thereafter, the image contours are extracted by a proposed curvature edge detection algorithm. Subsequently, the measurement location on the object is automatically selected based on the shape matching algorithm. The ball screw key parameters are computed by averaging multiple measurement methods to suppress random noise. Compared with the traditional method, this proposed method can be implemented for in-situ measurements with high efficiency.

The major contributions of the research are summarized below.

1) A vision-based method is developed for crucial parameters in-situ measurement of ball screws, where a shape matching algorithm is designed to automatically locate the contour features.
2) A curvature-based edge detection algorithm is proposed to extract the contours contained in the acquired digital images, where a fast mean curvature algorithm is employed to acquire the curvature information.

The remainder of the paper is structured as follows. Section II provides a description of the curvature-based edge detection method. Section III discusses the vision-based method for ball screw normal section inspection. Section IV describes the experiment on a ball screw. The result is listed in Section V. Section VI elaborates on the comparative trial and discussions. Section VII summarizes the main findings and conclusions of the study.

II. CURVATURE-BASED EDGE DETECTION

Edge detection is a fundamental element in image processing, machine vision, and computer vision, particularly in the areas of feature detection and extraction [19]. In this section, a novel curvature-based edge detection for ball screw inspection is proposed.

A. MEAN CURVATURE

Images can be embedded into a higher dimension to form surfaces. Furthermore, strong techniques from differential geometry may be utilized to analyze the surfaces. For an input image, $I(x, y)$, $(x, y, I(x, y))$ can be viewed as a three-dimensional surface [20]. It enables the employment of a specific differential geometry technique for image processing.

Curvature is an important definition in differential geometry which can be used to evaluate the deviation of a surface from a flat plane. A large curvature means that a surface has severe winding. Gaussian curvature (GC), mean curvature (MC), and principal curvature (PC) are the conventional curvatures used. Gong et al. [21] found that MC minimization results in few changes in the original image signal compared with GC and PC. Meanwhile, the MC is particularly interesting because it is related to minimal surfaces that commonly appear in the physical world. Similarity, for a given image, edge can be regard as a sharp change in image intensity. Therefore, in this research, mean curvature is used to identifying the contour information.

Gong and Sbalzarini [22] defined the eight directional curvatures (DCs) through arbitrary pixel points (the central black point in Figure 2), where two DCs represent the horizontal and vertical directions (Figure 2(b) and 2(f)), two DCs represent the directions inclined at by 45° and 135° (Figure 2(d) and 2(h)), and the remaining four DCs represent the four triangle zones that don't pass through the central point (Figure 2(a), 2(c), 2(g) and 2(e)). According to the Euler

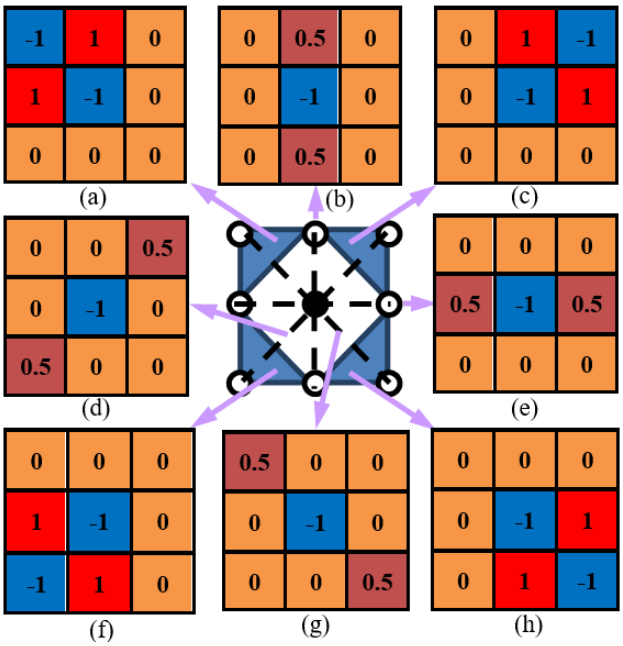

FIGURE 2. Curvature convolutional operation.

theorem, the MC calculation can be represented as a simple convolution operation (derivation details are found in [22]):

$$H = \begin{bmatrix} -\frac{1}{16} & \frac{5}{16} & -\frac{1}{16} \\ \frac{5}{16} & -1 & \frac{5}{16} \\ -\frac{1}{16} & \frac{5}{16} & -\frac{1}{16} \end{bmatrix} \otimes U \tag{1}$$

where $\otimes$ denotes the convolution operation, and $\boldsymbol{U}$ denotes the image gray information. Compared with the traditional MC calculation method, this novel method does not require second derivatives of the images. Meanwhile, without such twice-difference calculation, the computational efficiency can be also largely improved.

B. EDGE DETECTION ALGORITHM

It is commonly known that edge is a type of sharp change of image intensity. Generally, such changes can be detected by significant fluctuations in gradient magnitude [23], [24]. Correspondingly, the curvature at a point is a measure of the sensitivity of its tangent line to move the point to other nearby points, which similar to the definition of edge. Therefore, in this research, curvature is traying to detect the edge information of the image.

An ideal binary image is investigated in order to investigate the curvature-based edge detection algorithm. (details of the binary image are found in [25]). As shown in Figure 3(a), the blue color is used to light the best approximated pixels of the enveloping surface in the pixel matrix of the screen. Yellow illuminates the other region in the pixel matrix. After the convolution operation which is proposed in Eq. (1), the mean curvature can be calculated. Figure 3(b) is the corresponding MC along the white lines in Figure 3(a); the MC along the fifth line is presented in Figure 3(c). As can be seen in the local magnification, the corresponding MC oscillates with an amplitude that starts at zero, decreases, increases, and then decreases back to zero; the foregoing is similar to a wavelet function. According to Figure 3(c), MC is extremely sensitive to changes in image intensity and thus has a high potential for edge detection.

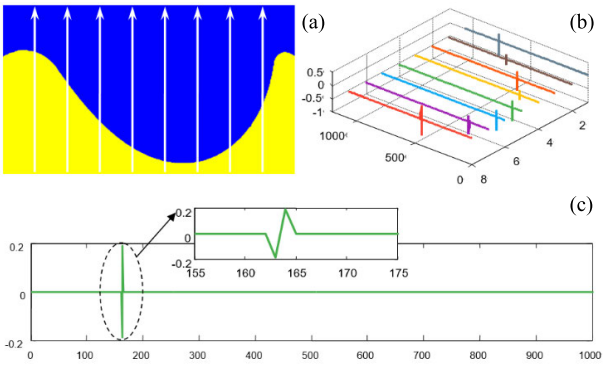

FIGURE 3. Edge detection in ideal situations.

An actual image intensity of the edge is shown in Figure 4. The figure shows that the edge pixel gray levels are not abruptly changed and distorted by distinct interference noise. The gray levels of the image on both sides of the edge permeate each other, and there is no distinct boundary between both edges of the image. Therefore, the MC sensitivity for edge detection has to be investigated. By applying the proposed convolution operation to an ideal binary image, the MC can be acquired. Figure 4(b) is the corresponding MC along the white lines in Figure 4(a). The MC along the fifth line is presented in Figure 4(c). As can be observed in this Figure, the corresponding MC also oscillates around the image edge. Compared with the ideal edge, the oscillation interval is enlarged in the actual image, a certain MC also occurs in the flat area. According to Figure 4, the MC seems to expedite the edge identification in the actual image.

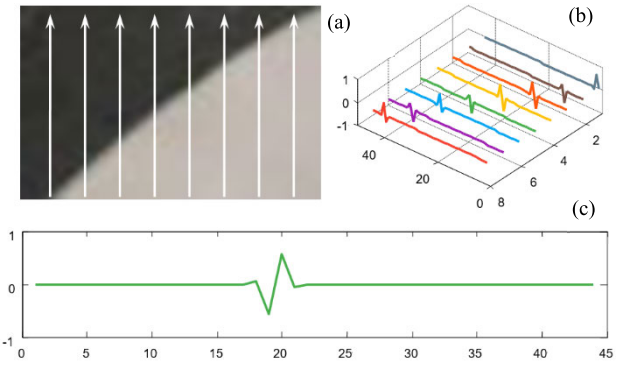

FIGURE 4. Edge detection for actual situation.

For an actual image generated by the imaging conditions and noise (fixed pattern noise, dark current noise, shot noise, amplifier noise, and quantization noise), the pixel gray

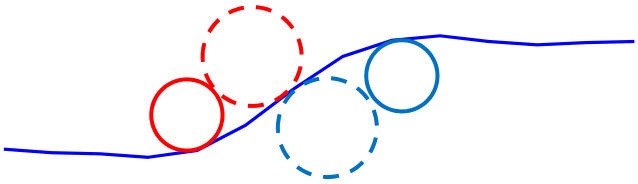

FIGURE 5. Curvature changes in actual edges.

level does not abruptly change, but gradually increases (or decreases). As can be observed in Figure 5, the gray level of the image (8-bit gray level) gradually increases. By analyzing the curvature change in the edge direction, it can be observed that the radius of curvature of the circle increases from small to maximum (red dotted line circle). Thereafter, the curvature changes direction, and the radius gradually decreases. It is noteworthy that the curvature changes abruptly (from the maximum to the minimum) along the reference line; this phenomenon is consistent with the definition of edge (the position where the gray level changes the most). Therefore, zero points of the curvature can be considered as the position of image edges.

According to the description above, the MC possesses good edge feature representation ability. Consequently, the curvature-based edge detection method can be explained below.

Step 1: Design the image acquisition system according to the measurement requirement.

Step 2: Capture the image based on the designed image acquisition equipment.

Step 3: Use the matrix presented in Section II-A to convolute the image and calculate the MC.

Step 4: Set the MC threshold ε and the edge width W_{edge} (edge width is employed for the edge verification, for example, there might be two edges in one row).

Step 5: Row scan the calculated MC matrix $\boldsymbol{H}$ to determine whether the matrix element satisfies the following conditions:

$$|H_{i,m}| \geq \varepsilon, |H_{j,m}| \geq \varepsilon \quad s.t. \begin{cases} H_{i,m} * H_{j,m} < 0 \\ |i-j| < W_{edge} \end{cases} \tag{2}$$

where i, j are the row numbers; m is the column number; range $[i{:}j, m]$ can be considered as the edge curve range. Its edge coordinate c_{edge} can be expressed as follows:

$$c_{edge} = (i+j)/2 \tag{3}$$

III. INSPECTION OF BALL SCREW NORMAL SECTION BY CURVATURE-BASED MACHINE VISION METHOD

Compared with the single-arc profile ball screw, the use of a double-arc profile ball screw is said to provide benefits such as stable contact change, improved transmission efficiency, and improved friction performance [26]. A double arc is a pair of arcs that are connected from beginning to end and are tangent to each other at the connection point. It has grooves at the bottom of the threaded groove, which can accommodate a certain amount of lubricating oil, reducing wear and improving the flow of the ball. An outline sketch of a double-arc profile ball screw is shown in Figure 6.

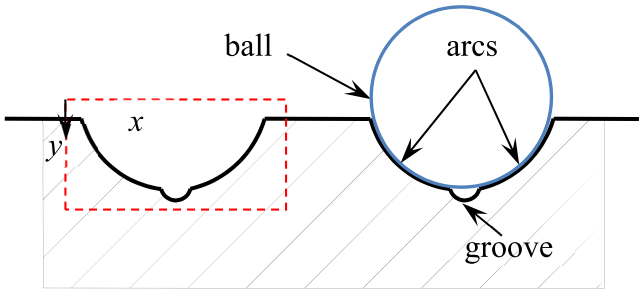

FIGURE 6. Double-arc profile ball screw.

The pitch, arc radius of the raceway, and ball eccentricity are the most important geometric parameters (parameters are illustrated in detail in Section IV-B). The manufacturing errors of these geometric parameters primarily impact the ball screw's bearing capacity, service life, and positioning accuracy. Therefore, a rapid and accurate ball screw measurement method is crucial.

A. SHAPE MATCHING ALGORITHM

It is supposed that finding the target location (region of interest, ROI) is the key function in automatic geometrical measurement. Recently, A multi-point matching algorithm and vision-based structural displacement measurement method have been suggested by Ye et al. [27]. Motivated by this approach, the authors propose a shape matching algorithm for the ball screw double-arc profile ball screw location. To find the target measurement location in the acquired image, a predesignated pattern is defined. The correlation coefficient score, which represents the matching extent between the pattern and the corresponding regions of the captured images, is computed.

As described in Figure 6, the region marked with a red rectangle is the theoretical contour curve. According to this curve and the magnification factors of the imaging system, the region pattern can be described as follows (assuming the pattern's origin is in the upper left corner):

$$\begin{bmatrix} p_x \\ p_y \end{bmatrix} = \begin{bmatrix} d_x \\ d_y \end{bmatrix} \begin{bmatrix} x_{Scale} & 0 \\ 0 & y_{Scale} \end{bmatrix} \tag{4}$$

where p_x and p_y are the pattern coordinate values; d_x and d_y are the designed coordinate values; x_{Scale} indicates the horizontal vision field magnification factor along the x direction, y_{Scale} indicates the horizontal vision field magnification factor along the x direction.

The region pattern is a $m \times$n matrix, but the obtain raw image is $M \times N$. Using the region pattern and the point (i, j), we get the correlation coefficient c(i, j) as follows:

$$c(i,j) = \sum_{x=0}^{M-1} \sum_{y=0}^{N-1} p(x,y) img(x+i, y+j) \tag{5}$$

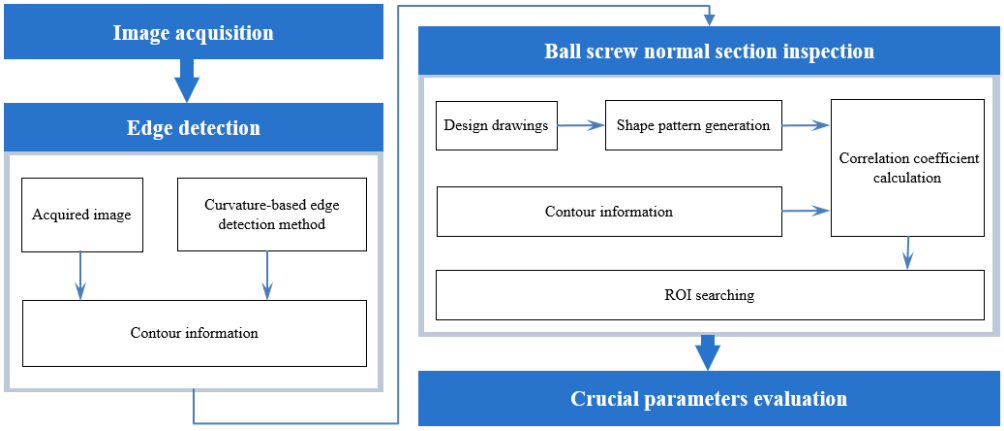

FIGURE 7. Flowchart of proposed method.

where $p(x, y)$ represents the normalized pattern, and $img(x, y)$ represents the normalized acquired image.

B. NORMAL SECTION INSPECTION

In terms of the region pattern, the two raceway arcs can easily be separated from the area of the determined object. According to the design principle, the center position and radius are indispensable. The least square method is a standard approach to the approximate solution of overdetermined systems; this means that the overall solution minimizes the sum of the squares of the errors made in the results of every single equation [28].

The general formula of the circular equation on the plane can be represented as:

$$x^2 + y^2 + ax + by + c = 0 \tag{6}$$

where $a = -2x_c$, $b = -2y_c$, and $c = x_c^2 + y_c^2 - r_c^2$, x_c and y_c locate the center position of the circle, r_c is the arc radius.

According to the least square theory, the objective function can be written as:

$$f(a, b, c) = \sum_{i=1}^{N} (x_i^2 + y_i^2 + ax_i + by_i + c)^2 \tag{7}$$

where (x_i, y_i) is the acquired raceway arc edge point numbering (N).

Let the three partial derivatives be zero.

$$\begin{bmatrix} \sum_{i=1}^{N} x_i^3 + \sum_{i=1}^{N} x_i y_i^2 \\ \sum_{i=1}^{N} x_i^2 y_i + \sum_{i=1}^{N} y_i^3 \\ \sum_{i=1}^{N} x_i^2 + \sum_{i=1}^{N} y_i^2 \end{bmatrix} + \begin{bmatrix} \sum_{i=1}^{N} x_i^2 & \sum_{i=1}^{N} x_i y_i & \sum_{i=1}^{N} x_i \\ \sum_{i=1}^{N} x_i y_i & \sum_{i=1}^{N} y_i^2 & \sum_{i=1}^{N} y_i \\ \sum_{i=1}^{N} x_i & \sum_{i=1}^{N} y_i & N \end{bmatrix} \begin{bmatrix} a \\ b \\ c \end{bmatrix} = \begin{bmatrix} 0 \\ 0 \\ 0 \end{bmatrix} \tag{8}$$

The above equations can be used to calculate the parameters a, b, and c. The radius of the raceway arc and its center can then be obtained.

The double arc profile ball screw is said to provide benefits like reliable contact change; hence, its ball eccentricity is crucial. As presented in Figure 6, it is indispensable to locate the ball center (marked with a solid blue line) in order to measure the ball eccentricity. The ball radius is given by the design drawings; therefore, this problem can be regarded as the simultaneous contact of a circle with two circles. After locating the ball center, the ball eccentricity and screw lead can be easy to calculate.

C. PROPOSED METHOD

In this paper, a novel curvature-based machine vision method for ball screw measurement is proposed. Figure 7 displays the proposed method's flowchart; relevant details are also described.

Step 1: Acquire the normal contour image of the measuring ball screws.

Step 2: Utilize the curvature-based edge detection method proposed in Section II to extract the image edge information.

Step 3: Using the design parameters, define the shape pattern; the object measurement location (region of interest, ROI) can be found automatically according to the proposed shape matching algorithm in Section III.

Step 4: The raceway arc radii and centers can be calculated using the standard least squares approach.

Step 5: Calculate the ball center based on the geometrical constraints (simultaneous contact of a circle with two arcs) and given ball radius.

Step 6: Calculate the average value through multiple measurements, the measuring errors can also be calculated accordingly.

IV. EXPERIMENTAL INVESTIGATION

In this section, according to the above-mentioned method, a ball screw measuring experiment is described.

A. EXPERIMENT SETUP

Figure 8 depicts the instrument configuration of the ball screw measurement system. The system consists of mechanical and

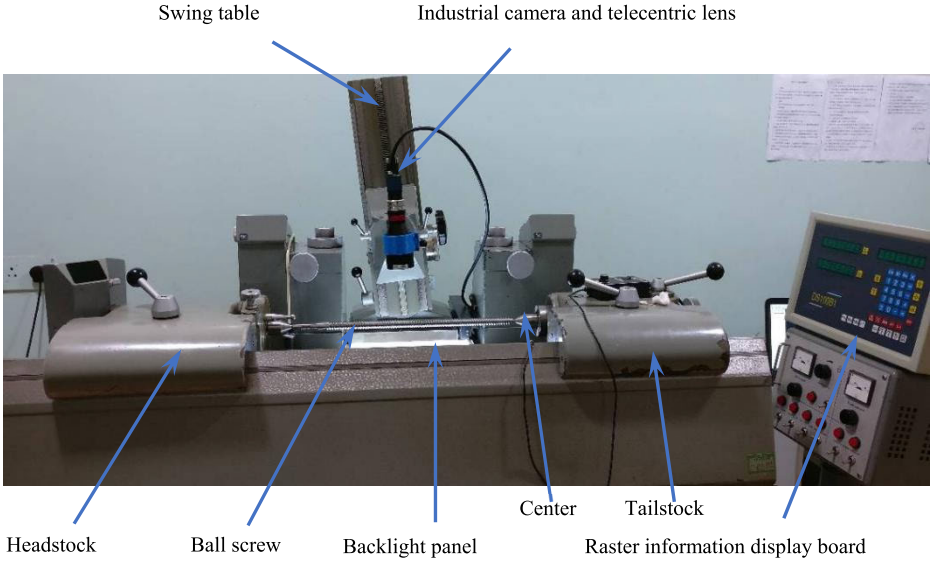

FIGURE 8. Measuring system configuration.

measuring parts. The mechanical part is similar to that of a traditional lathe. The headstock is attached to the left side of the bed. Tailstocks are able to slide on guides and are equipped with locking mechanisms. The distance between the tailstock and headstock is adjusted according to the length of the measured ball screw, and the tailstock is fixed onto the guide. The swing table contains a measurement sensor clamped to it, and the angle of the incline is adjusted manually according to the ball screw design parameter (lead angle) to ensure that the optical axis of the camera lens is perpendicular to the measurement plane. A backlight panel, an industrial camera, and a telecentric lens comprise the measurement component. To improve the contrast of measured contours, a customized backlight panel helped to set diffused backlighting. The ball screw's local images are captured using a telecentric lens. The raster information display board can be used to read the actual location information.

Before the capture of the image, the swing table incline angle is manually adjusted to the given lead angle according to the design parameters (the uncertainty is 30''). Therefore, the lens' optical axis is perpendicular to the normal section inspection of the ball screw. Besides, plane lighting is employed in this experiment. During the imaging process, the camera and plane lighting are individually positioned at two sides of the measurement plane. Table 1 lists the measurement system components.

B. BALL SCREW PARAMETERS

The measuring ball screw type is SW 059-01-301, which is produced by Shaanxi Hanjiang Machine Tool Co., Ltd, China. The position relationships of the thread profile's main geometrical parameters are shown in Figure 9 (without the lubrication groove) and listed in Table 2.

TABLE 1. Measuring system configuration.

No.	Component	Type
1	Camera	China Daheng Group, Inc, China, MER-1810-21U3C, 1/2.3 inch ON AR1820 CMOS, 1800 megapixels, 4912×3684, Mini USB3.0 interface
2	Lens	Shenzhen Shiqing Science Technology Limited Company, China, DTCM118-36-AL, working distance of 110mm
3	Plane lighting	Customized white plane lighting, with area of 200mm×200mm
4	Measuring bed	Leitz-Strasmann L020

TABLE 2. Measurement system components.

No.	Parameters	Symbol	Value
1	Lead angle		$5°40'50''$
2	Lead	L	5 mm
3	Lead precision		0.004 mm/2pi
4	Raceway radius	r_1, r_2	1.762 mm
5	Ball radius	ϕ_b	1.5875 mm
6	Outer diameter of screw	ϕ_O	$15.2^{-0.06}_{-0.11}$

C. EXPERIMENTAL PROCESS

As described in Figure 10, two different coordinate systems are defined; S_0-x_0y_0 is the static world coordinate system, and S_1-x_1y_1 is the moving coordinate system, which is fixed on the swing table. The position relationship between the two coordinate systems is determined by the grating location information from the raster information display board.

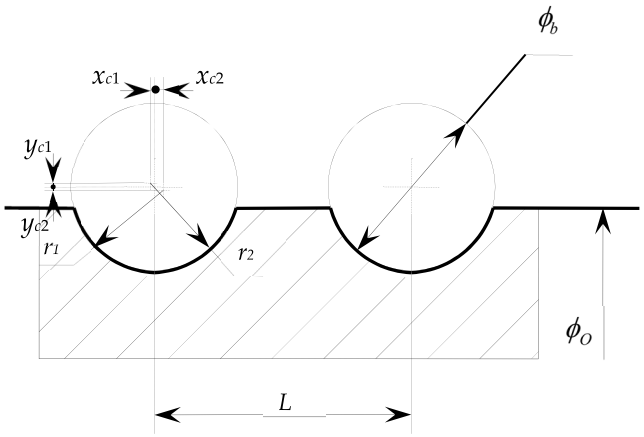

FIGURE 9. Thread profile.

Therefore, the actual location coordinate can be represented as:

$$\begin{bmatrix} x \\ y \end{bmatrix} = \begin{bmatrix} x_0 \\ y_0 \end{bmatrix} - \begin{bmatrix} x_1 \\ y_1 \end{bmatrix} \begin{bmatrix} \cos\theta & -\sin\theta \\ \sin\theta & \cos\theta \end{bmatrix} \begin{bmatrix} x_{Scale} \\ y_{Scale} \end{bmatrix} \quad (9)$$

where x and y are the actual coordinate points of the location, x_0 and y_0 denote the actual location information, which is read from the raster information display board, x_1 and y_1 are the pixel coordinate points in the acquired images, θ is the angle between the x direction in S_1-$x_1y_1$and $-x$ direction in S_0-x_0y_0 caused by the installation error, x_{Scale} indicates the horizontal vision field magnification factor along the x direction, y_{Scale} indicates the horizontal vision field magnification factor along the x direction.

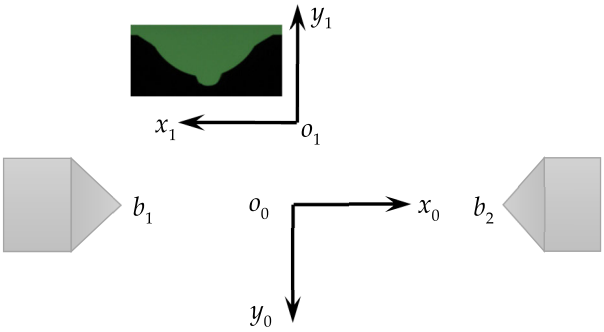

FIGURE 10. Coordinate system.

After calibration, the pixel equivalent is roughly 0.005 mm/pixel (the uncertainty is 1×10^{-3}mm). The industrial camera is utilized to take 20 photos continuously. Some samples of the acquired images are displayed in Figure 11. The samples are essentially identical to one another. Figure 11(a) and 11(b) are the initial two images captured; The difference between Figure 11(a) and 11(b) is shown in Figure 11(c), and the final two images are shown in Figure 11(d) and 11(e), and the difference between the final two images are shown in Figure 11(f). As shown in Figure 11,

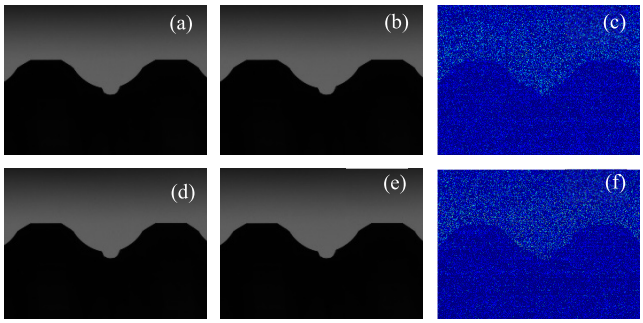

FIGURE 11. Acquired images.

even under identical imaging settings, the created noise in the sensing process has a significant negative impact on the image. In fact, any slight change can cause measurement result fluctuations because of camera resolution limitations. Consequently, the averaging multiple measurement methods is necessary to suppress random noise.

The processing of data for the first captured image (Figure 11(a)) is presented to further demonstrate the proposed method. The convolution operation is applied to the image; the mean curvature surf is shown in Figure 12(a), where the abrupt change in corresponding mean curvatures is always generated around the image edge; this verifies the validity of the proposed method. Using the suggested curvature-based edge detection approach described in Section II-B, the detected edge features are shown in Figure 12(b).

The region pattern (883 pixel×291 pixel) is applicable to Figure 12(b); Figure13(a) depicts the relating plane correlation coefficient, with the maximum of the correlation coefficient located in the white rectangular frame. The local magnification of the rectangle is shown in Figure 13(b). The magnification image indicates that the maximum correlation coefficient appears at the coordinate point (439, 436), which means that this coordinate is most probably the origin of the ROI.

Therefore, the ROI is the rectangular area located between point (439, 436), the upper-left corner, and point (1432, 727), the lower-right corner. The extracted ROI is shown in Figure 14. According to the predefined pattern, Separating the two raceway arcs (dashed rectangle areas in Figure 14) from the ROI is convenient. Using the proposed normal section inspection method in Section III-B, the raceway arcs and center distance can be estimated.

V. RESULTS

As presented in the measurement procedure, the experiment adopts the averaging multiple measurement methods to suppress random noise. Table 3 sums up the experimental results. The predicted mean values for the two raceway arcs are 1.7462 mm, and 1.7342 mm, it computed standard deviations are 0.0033 mm, and 0.0047 mm. The center distance is guesstimated to be 0.2349 mm, and its standard deviations is 0.0032mm.

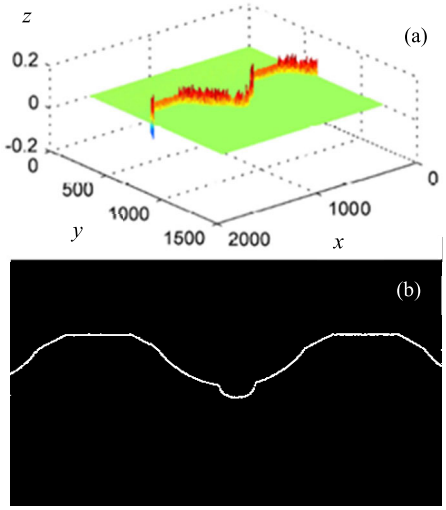

FIGURE 12. Curvature-based edge detection.

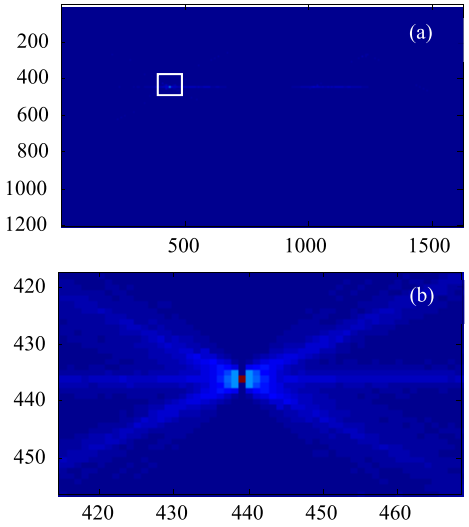

FIGURE 13. ROI location.

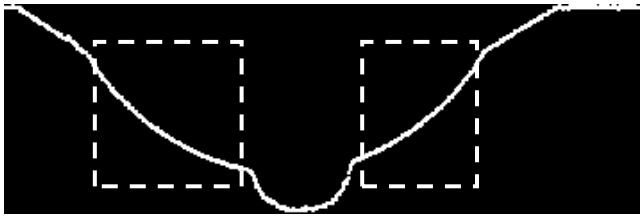

FIGURE 14. Extracted ROI.

In reality, contact measurement is regarded as the most reliable measuring method; it may serve as a benchmark by which other measurement methods can be measured. The ball screw contact measurement is performed using the Hommel Etamic T8000 (an instrument for combined roughness and contour measurement; measurement resolution: 0.01 μm) to further validate the measurement results. The measurement results are shown in Figure 15. According to the results

TABLE 3. Experimental results.

No.	r1 / mm	r2 / mm	Distance / mm
1	1.7389	1.7403	0.2337
2	1.7483	1.7375	0.2376
3	1.7419	1.7278	0.2282
4	1.7468	1.7322	0.2343
5	1.7476	1.7312	0.2348
6	1.7487	1.7281	0.2331
7	1.7485	1.7360	0.2378
8	1.7440	1.7292	0.2299
9	1.7510	1.7342	0.2380
10	1.7422	1.7301	0.2297
11	1.7461	1.7297	0.2319
12	1.7483	1.7375	0.2376
13	1.7485	1.7360	0.2378
14	1.7441	1.7447	0.2409
15	1.7481	1.7315	0.2346
16	1.7411	1.7417	0.2357
17	1.7476	1.7312	0.2348
18	1.7478	1.7329	0.2356
19	1.7437	1.7372	0.2351
20	1.7510	1.7342	0.2380
Mean	1.7462	1.7342	0.2349
S.D.	0.0033	0.0047	0.0032

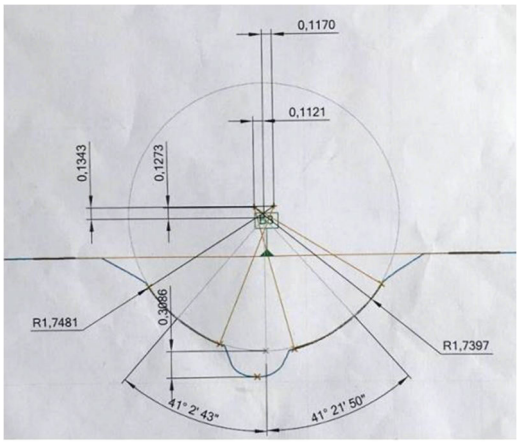

FIGURE 15. Contact measurement result.

TABLE 4. Result comparison.

	r_1 / mm	r_2 / mm	Distance / mm
Contact measurement	1.7481	1.7397	0.2291
Proposed method	1.7462	1.7342	0.2350
Absolute error	0.0019	0.0055	0.0059
Relative error	0.1900%	0.5500%	0.5900%

presented in Table 4, the absolute measurement errors of the two raceway arcs are assessed to be 0.0019 mm, and 0.0055 mm, and their relative errors are estimated to be

TABLE 5. Contrast experiment results.

No.	Method	Absolute error				Computing time / s
		r1 / mm	r2 / mm	Distance / mm	Average / mm	
1	Proposed method	0.0019	0.0055	0.0059	0.0044	0.0053
2	Prewitt	0.0144	0.0008	0.0027	0.0060	0.0080
3	Sobel	0.0161	0.0006	0.0037	0.0068	0.0089
4	Canny	0.0129	0.0005	0.0014	0.0050	0.1062
5	log	1.2692	1.3008	1.2472	1.2724	0.0433

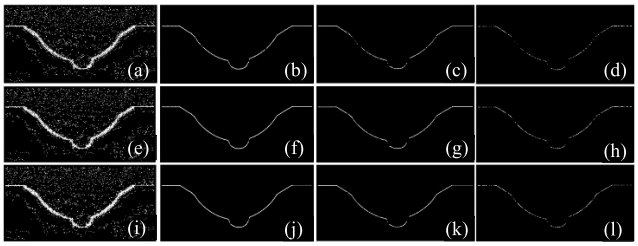

FIGURE 16. Comparative experiment results in different parameters. (a) obtained edge when MC threshold is 0.1 × maximum of the curvature and edge width is 3 (b) obtained edge when MC threshold is 0.2 × maximum of the curvature and edge width is 3 (c) obtained edge when MC threshold is 0.3 × maximum of the curvature and edge width is 3 (d) obtained edge when MC threshold is 0.4 × maximum of the curvature and edge width is 3 (e) obtained edge when MC threshold is 0.1 × maximum of the curvature and edge width is 4 (f) obtained edge when MC threshold is 0.2 × maximum of the curvature and edge width is 4 (g) obtained edge when MC threshold is 0.3 × maximum of the curvature and edge width is 4 (h) obtained edge when MC threshold is 0.4 × maximum of the curvature and edge width is 4 (i) obtained edge when MC threshold is 0.1 × maximum of the curvature and edge width is 5 (j) obtained edge when MC threshold is 0.2 × maximum of the curvature and edge width is 5 (k) obtained edge when MC threshold is 0.3 × maximum of the curvature and edge width is 5 (l) obtained edge when MC threshold is 0.4 × maximum of the curvature and edge width is 5.

0.19% and 0.55%. The center distance's absolute measurement errors are estimated to be 0.0059 mm, while its relative errors are predicted to be 0.59%.

VI. DISCUSSIONS

To further evaluate the applicability of the proposed curvature-based method, in this section, the parameter setting influence and the comparative experiment are investigated.

A. INFLUENCE OF DIFFERENT SETTING PARAMETER

To deeply investigate the influence of the setting parameters (MC threshold ε and the edge width W_{edge} in Section II) in the proposed method, a series of comparative experiments are conducted. The corresponding results are shown in Figure, where the horizontal direction indicates the change of the MC threshold and the vertical direction represents the change of edge width.

As can be seen in the figure, with the increase of the MC threshold, the proposed method tends to export much edge information. Meanwhile, the edge width is more like a filter. With the increase of edge width, the proposed method will preserve more edge features. However, more edge features might also generate fake edges. Accordingly, the results demonstrate that the appropriate selection of setting parameters if of great importance for better edge detection. Based on the results listed above, in this research, MC threshold and the edge width are chosen as 0.2 × maximum of the curvature and 4 respectively.

B. CONTRAST EXPERIMENTS

To investigate the superiority of the proposed method, the contrast experiments are conducted. The measuring errors using different edge detection method is shown in Table 5. All the experiments are performed under Win 10 environment on a machine with CPU Intel Core i5-8500 @ 3.00 GHz. The computing time during the experiment is also recorded. As can be seen in the table, the proposed curvature-based method recorded better performance. While the proposed method and Soble method receive better computational efficiency exhibition.

VII. CONCLUSION

In this paper, a measurement method based on machine vision is proposed to realize the highly accurate measurements of ball screws. In the contour extraction phase, a curvature-based edge detection method is successfully proposed. Combined with the shape matching algorithm and averaging multiple measurement methods, the ball screw key parameters are successfully measured. The major findings of this work can be summarized below:

(1) The proposed method is shown to be an efficacious tool for evaluating ball screw manufacturing precision. The proposed method can be employed to measure ball screws in situ without trying to remove any workpiece. Compared with the traditional contact measurement method, the calculated absolute measurement errors of the two raceway arcs are assessed to be 0.0019 mm, and 0.0055 mm, and the center distance's absolute measurement errors are estimated to be 0.0059 mm; the relative error maximum value is 0.59%.

(2) In order to minimize the influence of generated noise in the imaging process, the averaging multiple measurement methods are adopted to suppress random noise. According to the contrast experiment, this method can effectively reduce the errors caused by image pixel gray level variation.

The proposed method is still far from online rapid measurement due to the restriction of equipment parameters (frame rate, 21 frames per second). The proposed method will also be used in the next step to control active control operations during the machining process. The uncertainty analysis of the proposed method in different workpiece dimension is also worth further exploration.

ACKNOWLEDGMENT

The author Yijia Chen thanks Shaanxi Hanjiang Machine Tool Company Ltd., China, for providing equipment for this research and the technical support from Dr. Weifang Sun (Member, IEEE). *(Yijia Chen, Yao Yao, and Hao Yang contributed equally to this work.)*

REFERENCES

[1] H.-C. Lee, Y.-C. Chang, and Y.-S. Huang, "A reliable wireless sensor system for monitoring mechanical wear-out of parts," *IEEE Trans. Instrum. Meas.*, vol. 63, no. 10, pp. 2488–2497, Oct. 2014, doi: 10.1109/TIM.2014.2312498.

[2] C. Zhang and Y. Chen, "Tracking control of ball screw drives using ADRC and equivalent-error-model-based feedforward control," *IEEE Trans. Ind. Electron.*, vol. 63, no. 12, pp. 7682–7692, Dec. 2016, doi: 10.1109/TIE.2016.2590992.

[3] K.-C. Fan and M.-W. Liang, "Development of an automatic cumulative-lead error measurement system for ballscrew nuts," *Int. J. Adv. Manuf. Technol.*, vol. 72, nos. 1–4, pp. 17–23, Apr. 2014, doi: 10.1007/s00170-013-4905-1.

[4] Z.-D. Zhou, L. Gui, Y.-G. Tan, M.-Y. Liu, Y. Liu, and R.-Y. Li, "Actualities and development of heavy-duty CNC machine tool thermal error monitoring technology," *Chin. J. Mech. Eng.*, vol. 30, no. 5, pp. 1262–1281, Sep. 2017, doi: 10.1007/s10033-017-0166-5.

[5] N. Riaz, S. I. A. Shah, F. Rehman, and M. J. Khan, "An intelligent hybrid scheme for identification of faults in industrial ball screw linear motion systems," *IEEE Access*, vol. 9, pp. 35136–35150, 2021, doi: 10.1109/ACCESS.2021.3062496.

[6] X. Zhang, J. Zhang, W. Zhang, T. Liang, H. Liu, and W. Zhao, "Integrated modeling and analysis of ball screw feed system and milling process with consideration of multi-excitation effect," *Mech. Syst. Signal Process.*, vol. 98, pp. 484–505, Jan. 2018, doi: 10.1016/j.ymssp.2017.05.011.

[7] S. Sandu, N. Biboulet, D. Nelias, and F. Abevi, "An efficient method for analyzing the roller screw thread geometry," *Mechanism Mach. Theory*, vol. 126, pp. 243–264, Aug. 2018, doi: 10.1016/j.mechmachtheory.2018.04.004.

[8] G.-H. Feng and C.-C. Wang, "Examining the misalignment of a linear guideway pair on a feed drive system under different ball screw preload levels with a cost-effective MEMS vibration sensing system," *Precis. Eng.*, vol. 50, pp. 467–481, Oct. 2017, doi: 10.1016/j.precisioneng.2017.07.001.

[9] G. Liu, H. Luo, Y. Zhang, J. Qian, J. Liu, and C. Liu, "Pulse electrochemical machining of large lead ball nut raceway using a spherical cathode," *Int. J. Adv. Manuf. Technol.*, vol. 85, nos. 1–4, pp. 191–200, Jul. 2016, doi: 10.1007/s00170-015-7937-x.

[10] W. Sun, B. Yao, B. Chen, Y. He, X. Cao, T. Zhou, and H. Liu, "Noncontact surface roughness estimation using 2D complex wavelet enhanced ResNet for intelligent evaluation of milled metal surface quality," *Appl. Sci.*, vol. 8, no. 3, p. 381, Mar. 2018, doi: 10.3390/app8030381.

[11] A. N. André, P. Sandoz, B. Mauzé, M. Jacquot, and G. J. Laurent, "Robust phase-based decoding for absolute (X, Y, Θ) positioning by vision," *IEEE Trans. Instrum. Meas.*, vol. 70, pp. 1–12, 2021, doi: 10.1109/TIM.2020.3009353.

[12] W. Sun, B. Chen, B. Yao, X. Cao, and W. Feng, "Complex wavelet enhanced shape from shading transform for estimating surface roughness of milled mechanical components," *J. Mech. Sci. Technol.*, vol. 31, no. 2, pp. 823–833, Feb. 2017, doi: 10.1007/s12206-017-0134-0.

[13] F. Carvajal-Ramírez, A. D. Navarro-Ortega, F. Agüera-Vega, P. Martínez-Carricondo, and F. Mancini, "Virtual reconstruction of damaged archaeological sites based on unmanned aerial vehicle photogrammetry and 3D modelling. Study case of a southeastern Iberia production area in the bronze age," *Measurement*, vol. 136, pp. 225–236, Mar. 2019, doi: 10.1016/j.measurement.2018.12.092.

[14] C.-Y. Liu and T.-P. Yen, "Digital multi-step phase-shifting profilometry for three-dimensional ballscrew surface imaging," *Opt. Laser Technol.*, vol. 79, pp. 115–123, May 2016, doi: 10.1016/j.optlastec.2015.12.001.

[15] C. Wu, P. Yang, T. Lei, D. Zhu, Q. Zhou, and S. Zhao, "A teaching-free welding position guidance method for fillet weld based on laser vision sensing and EGM technology," *Optik*, vol. 262, Jul. 2022, Art. no. 169291, doi: 10.1016/j.ijleo.2022.169291.

[16] R. Xiang, W. He, X. Zhang, D. Wang, and Y. Shan, "Size measurement based on a two-camera machine vision system for the bayonets of automobile brake pads," *Measurement*, vol. 122, pp. 106–116, Jul. 2018, doi: 10.1016/j.measurement.2018.03.017.

[17] Y. Gong and E. J. Seibel, "Three-dimensional measurement of small inner surface profiles using feature-based 3-D panoramic registration," *Opt. Eng.*, vol. 56, no. 1, Jan. 2017, Art. no. 014108, doi: 10.1117/1.OE.56.1.014108.

[18] W. K. Lee, M. M. Ratnam, and Z. A. Ahmad, "Detection of chipping in ceramic cutting inserts from workpiece profile during turning using fast Fourier transform (FFT) and continuous wavelet transform (CWT)," *Precis. Eng.*, vol. 47, pp. 406–423, Jan. 2017, doi: 10.1016/j.precisioneng.2016.09.014.

[19] A. F. John, L. Bai, Y. Cheng, and H. Yu, "A heuristic algorithm for the reconstruction and extraction of defect shape features in magnetic flux leakage testing," *IEEE Trans. Instrum. Meas.*, vol. 69, no. 11, pp. 9062–9071, Nov. 2020, doi: 10.1109/TIM.2020.2998561.

[20] C. Brito-Loeza, K. Chen, and V. Uc-Cetina, "Image denoising using the Gaussian curvature of the image surface," *Numer. Methods for Partial Differ. Equ.*, vol. 32, no. 3, pp. 1066–1089, May 2016, doi: 10.1002/num.22042.

[21] Y. Gong, X. Hou, F. Li, and G. Qiu, "Image filtering with generic geometric prior," *IEEE Access*, vol. 6, pp. 54320–54330, 2018, doi: 10.1109/ACCESS.2018.2871829.

[22] Y. Gong and I. F. Sbalzarini, "Curvature filters efficiently reduce certain variational energies," *IEEE Trans. Image Process.*, vol. 26, no. 4, pp. 1786–1798, Apr. 2017, doi: 10.1109/TIP.2017.2658954.

[23] A. H. Abdel-Gawad, L. A. Said, and A. G. Radwan, "Optimized edge detection technique for brain tumor detection in MR images," *IEEE Access*, vol. 8, pp. 136243–136259, 2020, doi: 10.1109/ACCESS.2020.3009898.

[24] Y. Zhang, Y. Shi, L. Ma, J. Wu, L. Wang, and H. Hong, "Blind natural image deblurring with edge preservation based on L_0-regularized gradient prior," *Optik*, vol. 225, Jan. 2021, Art. no. 165735, doi: 10.1016/j.ijleo.2020.165735.

[25] Z. Shen, B. Yao, W. Teng, W. Feng, and W. Sun, "Generating grinding profile between screw rotor and forming tool by digital graphic scanning (DGS) method," *Int. J. Precis. Eng. Manuf.*, vol. 17, no. 1, pp. 35–41, Jan. 2016, doi: 10.1007/s12541-016-0005-0.

[26] L.-X. Zhou and P.-Y. Li, "Finite element analysis of the axial stiffness of a ball screw," *IOP Conf. Ser., Mater. Sci. Eng.*, vol. 372, Jun. 2018, Art. no. 012023, doi: 10.1088/1757-899X/372/1/012023.

[27] X. W. Ye, T.-H. Yi, C. Z. Dong, and T. Liu, "Vision-based structural displacement measurement: System performance evaluation and influence factor analysis," *Measurement*, vol. 88, pp. 372–384, Jun. 2016, doi: 10.1016/j.measurement.2016.01.024.

[28] L. Zhao, H. Feng, and Q. Rong, "A novel non-contact measuring system for the thread profile of a ball screw," *Mech. Sci.*, vol. 9, no. 1, pp. 15–24, Jan. 2018, doi: 10.5194/ms-9-15-2018.

YIJIA CHEN was born in China. She is currently pursuing the degree in intelligent manufacturing with the College of Mechanical and Electrical Engineering, Wenzhou University. Her main research interests include machine vision and condition monitoring.

YAO YAO was born in China, in 2001. He is currently pursuing the degree in intelligent manufacturing with the College of Mechanical and Electrical Engineering, Wenzhou University. His main research interests include signal processing and measurement.

HAO YANG was born in China. He is currently pursuing the degree in intelligent manufacturing with the College of Mechanical and Electrical Engineering, Wenzhou University. His main research interests include measurement and instrument.

YUE WU was born in China. She is currently pursuing the degree in logistics engineering with the College of Urban Transportation and Logistics, Shenzhen Technology University. Her main research interests include condition monitoring and artificial intelligence.

KUNPENG ZHANG was born in China. He received the Ph.D. degree in mechanical engineering from Xiamen University, in 2021. He has published around ten peer-reviewed publications. He is mainly engaged in the micro/nano 3D printing and digital signal processing.

XIAOMING PAN was born in Wenzhou, Zhejiang, China, in 1980. He received the B.S. degree from the Zhejiang University of Technology, Hangzhou, China, in 2004, and the M.S. degree from Jiangsu University, Zhenjiang, in 2014.

He is currently a Senior Experimentalist with the College of Mechanical and Electrical Engineering, Wenzhou University. He has published more than ten peer-reviewed articles in international journals. His research interests include cutting processing and processing analysis.